Journal of Orthopaedic Translation 38 (2023) 12–22

Contents lists available at ScienceDirect

Journal of Orthopaedic Translation

journal homepage: www.journals.elsevier.com/journal-of-orthopaedic-translation

Scoliosis assessment tools to reduce follow-up X-rays

Alexander T.D. Grünwald [a], Susmita Roy [a], Renée Lampe [a,b,*]

[a] Technical University of Munich, School of Medicine, Klinikum rechts der Isar, Orthopaedic Department, Research Unit of the Buhl-Strohmaier Foundation for Cerebral Palsy and Paediatric Neuroorthopaedics, Munich, Germany
[b] Markus Würth Professorship, Technical University of Munich, Munich, Germany

ARTICLE INFO

Keywords:
Body scanner
Finite element method
Non-invasiv
Scoliosis

ABSTRACT

Purpose: Clinical examinations of scoliosis often includes X-rays. Regular clinical monitoring is recommended in particular at young age, because of the high risk of progression during periods of rapid growth. Supplementary methods free of ionizing radiation thus could help to reduce the potential risk of ionizing radiation related health problems.
Methods: Twelve 3D scan images from female and male patients with different types and severities of spinal deformations were analysed using body scanner image analysis tools. The scan images were captured with a 3D body scanner, which used an infrared sensor and a video camera. To calculate and compare with the patient's specific spinal deformations, simulations based on finite elements methods were performed on biomechanical models of ribcage and spinal column.
Results: The methods and parameters presented here are in good agreement with corresponding X-rays, used for comparison. High correlation coefficients of $\|\rho_s\| \geq 0.87$ between Cobb angle and lateral deviation, as well as between Cobb angle and rotation of the vertebrae, indicate that the parameters could provide supplementary informations in the assessment of spinal deformations. So-called apex angles, in addition introduced to relate the results of the present method with Cobb angles, show strong correlations of $\|\rho_s\| \geq 0.68$ and thus could be used for comparison in later follow-up examinations.
Conclusion: The user-friendly 3D body scanner image analysis tools enable orthopaedic specialists to simulate, visualize and inspect patient's specific spinal deformations. The method is intended to provide supplementary information in complement to the Cobb angle for the assessment of spinal deformations in clinical daily routine and might have the potential to reduce X-rays in follow-up examinations.
The Translational Potential of this article: The study presents a new method, based on 3D body scanner images and biomechanical modelling, that has the potential to reduce X-rays when monitoring scoliosis especially in young patients.

1. Introduction

Idiopathic scoliosis is a three dimensional deformation of the spinal column by lateral deviation, and rotation and torsion around the vertical axis of the individual vertebral bodies [1–3]. The lateral curvature of the spine, measured by Cobb angle, has to be more than 10° to be classified as scoliosis.

In a clinical examination a thoracic scoliosis presents itself in a rib hump with posterior elevation on the convex side and a flattening on the concave side, due to the rotation of the vertebral bodies and the resulting distortion of attached ribs. In the case of lumbar scoliosis, waist asymmetry and a lumbar bulge are the most prominent signs. In general, scoliosis has no symptoms at early stage. For example, female adolescents can show breast asymmetry due to scoliosis, which is reflected in a change in the back contour at the upper part of body. Depending on the spinal curvature, various types of treatments are recommended, including physical therapy, brace treatment, or surgery [4]. The presence of scoliosis in adolescent, in general, has a high risk of progression. Therefore, it is recommended that in particular young patients diagnosed with scoliosis do have regular clinical follow-up examinations, according to their bone growth. Follow-up examinations sometimes include X-ray of the spine and thus recurred exposure to ionizing radiation. For diagnosis of scoliosis, in particular at the first appointment, X-rays are essential and gold-standard. However, in follow-up examinations it is

* Corresponding author. Klinikum rechts der Isar, Ismaninger Strasse 22, 81675, Munich, Germany.
E-mail address: renee.lampe@tum.de (R. Lampe).

https://doi.org/10.1016/j.jot.2022.07.010
Received 2 February 2022; Received in revised form 8 June 2022; Accepted 26 July 2022

desirable to minimize the exposure to radiation, particularly at young age, since a single X-ray image is associated with exposure to radiation of 400–800 μGy [5], depending on the body mass index. Although Oakley et al. [6] stated theoretically that the cumulative radiation doses from scoliosis related X-ray examinations do not reach the critical value of carcinogenic risk, there is no doubt that in paediatric radiology a high level of attention is always paid to whether an X-ray examination is absolutely necessary, or not. Children in particular have high growth potential, a long life expectancy and radiation-sensitive tissue. For this reason, restrictive handling of ionizing radiation is required in this age group [7]. Therefore, there is a need for non-invasive, radiation-free techniques that can be used more frequently in daily routine to support medical observations during follow-up examinations of scoliosis [8–10].

A number of different non-invasive, contactless techniques and methods free of ionizing radiation have been developed for this purpose [11–15]. By now there are several types of fast and contactless body scanners available that provide precise 3D images of the outer body contours in order to visualize and capture asymmetries from externally visible deformities in the assessment of idiopathic scoliosis [16]. In parallel various techniques have been developed that automatically, or semi-automatically, recognize certain body points and characteristic features due to scoliosis. These techniques include different surface topography methods using stereo cameras [17] Moiré-fringe mapping [18] and raster stereography [15]. The majority of these systems focuses on asymmetries of the outer body contours in order to deduce the shape and curvature of the spinal column from anatomical feature points [19,20]. These techniques, however, often need additional markers at certain body points and do not provide internal anatomical information about the spine. Especially they do not yield much information about the rotation of vertebral bodies. In complement, efforts have been made to reduce the radiation dose by using a scanning radiography imaging system, like EOS, for the evaluation of scoliosis. Recent studies have shown that this system can significantly reduce the patient's radiation exposure in comparison with conventional radiographs with similar image quality [21,22]. However, the EOS system is relatively expensive, not completely ionization radiation free and difficult to use for children with disabilities, though, as they need to adopt and maintain a stable posture and position [22]. 3D body scanners are in particular used in medical studies to build anthropometric databases [23,24]. Recently, a portable, electronic device, based on ergonomics (human factors), has been developed as a non-invasive tool for early detection of adolescent scoliosis [25].

Regardless of different approaches, the ultimate goal of all these developments is to reduce the risk of radiation-related secondary diseases from multiple x-rays when assessing scoliosis in children, especially during sensitive phases of growth. To our knowledge, the pathogenesis of scoliosis is still unclear and it is assumed to be a multi factorial disease. Irrespective of the cause, the progression of scoliosis is a matter of biomechanics [26] and the axial rotations of the vertebral bodies around the vertical body axis and their correlation with lateral deviations have significant effects on the initiation and progression of scoliosis. Biomechanical modelling of the human spine, using Finite Element Methods (FEM), has therefore gained a lot of attention and many FEM models have been developed for the thoracic, lumbar and cervical spine [27–30]. To adapt a FE model to the patient specific characteristics, in general, a precise estimation of the model parameters is required and these methods thus are potentially more accurate. In addition, FE analysis (FEA) allows to analyse the effects of external stress and internal strain on the spine. FEA can thereby possibly help to (further) reveal the aetiology of scoliosis and the biomechanics of a progressive scoliosis, as well as improve the understanding of the initial formation of a scoliosis from a mechanical point of view [31].

Patients with cerebral palsy (CP) have a higher incidence of developing scoliosis than others [32]. Previously a body scanner system has been developed especially considering examination requirements for patients with CP [33]. The body scanner provides a 3D image of the patient's torso. In the present study a user-friendly graphical user interface (GUI) have been developed to allow orthopaedic specialists to visualize and analyse patient's specific spinal deformations due to scoliosis from the torso image. The GUI allows for macroscopic FEM simulations of individual spinal deformations on a biomechanical model of the spine and ribcage, built with CAD. The resulting, accordingly deformed model is fitted into the 3D torso image, captured by the body scanner. The best configuration is found by visually fitting several cuts of the model into the corresponding body contours from different perspectives. This configuration can then be used at follow-up examinations for initial setting and comparison with previous results, revealing changes in the patients scoliotic spine deformity without further X-rays, provided that no other indications and conditions requiring an X-ray.

2. Material and methods

2.1. Material

In this study 10 patients (5 female and 5 male), aged 11–50 years (average: 21 years), were analysed with methods presented hereinafter. All patients showed signs of spinal deformation. Some patients were affected by neurogenic scoliosis, due to neuromuscular imbalance from CP, while others were diagnosed with idiopathic scoliosis. All patients, including those with neurogenic scoliosis, were able to stand upright without support. X-rays were available for all patients at the time of body scan.

The previously developed body scanner system is equipped with an infrared depth sensor and a RGB video camera. Using computer vision algorithms, the system provides a true colour 3D image of the patients torso upon scanning [33,34]. It is thus non-invasive and ionizing radiation free. Moreover the scanner is mobile and can be easily packed and set up at other places than the hospital. Patients were asked to stand still and upright, with their arms slightly abducted, during the scanning process of less than 10 seconds.

Ribcage models of female and male were designed [35], according to various geometry parameters taken from literature, using Computer Aided Design (CAD) methods. From the different geometries for female and male we have then build basic models for FEM simulations with FEBio, a software suite for biomechanics [36]. The models essentially are made of rigid and thus non-deformable vertebral bodies and non-linear, according to a neo-Hookean solid [37,38], elastic ribs attached to them. Non-linear elastic intervertebral discs further give flexibility to the spinal column [35]. The basic material properties, namely the modulus of elasticity and the Poisson's ratio, for the non-linear elastic components of the model are given in Table 1. Since the stiffness varies with age [39–41], the corresponding Young's moduli were considered as a function of age [42]. The densities were estimated to $1.0 \cdot 10^3$ kg/m^3 in broad accordance with corresponding parameters in other studies [43–47]. For the simulations the models were meshed into 4-node linear tetrahedral finite elements. Microscopic biomechanical properties were not considered in the present study.

2.2. Methods

Fig. 1a shows a screenshot of the GUI of the body scanner image analysis tools. The main window is separated into three sections: X-ray (X), images extracted from 3D body scanner and spinal column and ribcage models simulations (B) and simulation settings (S), from left to right.

Table 1
Material properties of the elastic model components.

Component:	Young's modulus (GPa):	Poisson's ratio:
Costal cartilage	$10.5 \cdot 10^{-3}$ [52]	0.2
Intervertebral disk	$30.9 \cdot 10^{-3}$ [41]	0.45 [46,47]
Rib	$6.71 \cdot$ (age in years)$^{0.2}$ [42]	0.3

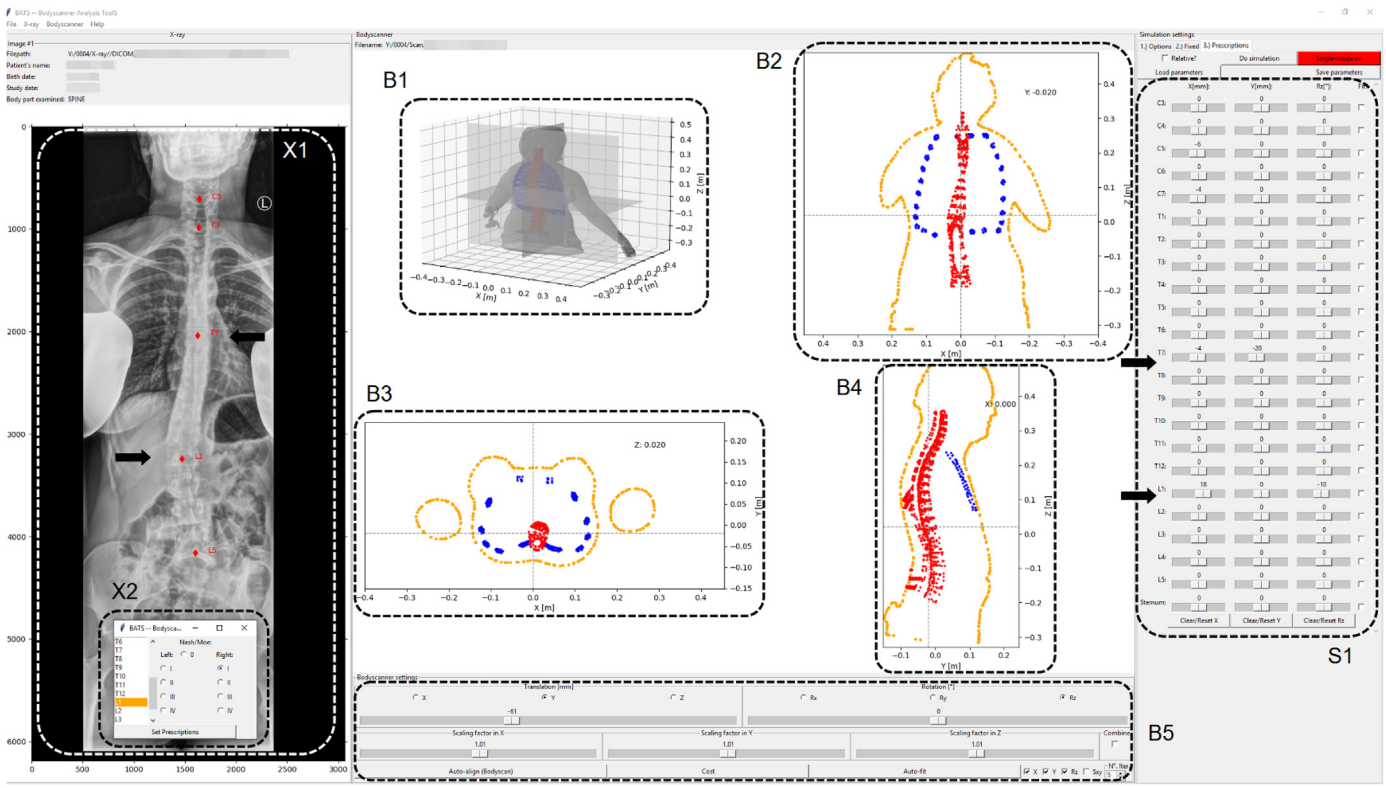

Figure 1. Fig. 1a: Screenshot of the graphical user interface (GUI) of the body scanner image analysis tools. The GUI is separated in three sections: X-ray 'X' (left), images extracted from 3D body scanner and spinal column and ribcage models simulations 'B' (centre) and model simulation settings 'S' (right). Further details are described in the text. Fig. 1b: Screenshot of simulation settings 2nd tab: Translational and rotational degrees of freedom can be confined/fixed individually for all vertebral bodies.

To simulate the patient's specific deformation of the vertebral column, here at the example of a female patient with right convex thoracolumbar scoliosis, characteristic feature points along the vertebral column were marked (diamond symbols) on the X-ray, using an in-built pop-up tool (shown in the inset X2). Important markers were in general the positions of vertebral bodies that define the shape of the spinal column, for instance the apex level(s) and the beginning/end of lateral curvature(s). The required marker at L5 was used as reference point to find out the lateral translation. Additionally markers at the cervical spine helped to scale the model according to the patient's individual height and could be used for orientation of the vertical body axis later on. The lateral distances of all the markers relative to L5 were then transferred to the simulation section (S) as initial simulation settings for the lateral deviations (Tx) of the corresponding vertebrae. Besides the lateral positions, each marker on the X-ray (X1) could be associated with a degree of rotation around the vertical axis, after Nash-Moe index [48] (cf. X2). The corresponding angular rotations (Rz) were also transferred to the simulation settings. In the example shown here these were in lateral translation 18 mm at L1, -4 mm at T7 and C7, and -6 mm at C5. In angular rotation it was -10° only at L1. Sliders for lateral (Tx) and anterior-posterior (Ty) deviation, as well as rotations (Rz) around the vertical body axis, further allowed to individually adjust any of these settings for any of the vertebral bodies between C3 and L5. In practice, however, it was sufficient to define the deviations and rotation only at a couple of feature points along the vertebral column, for instance the apex levels of the main curvature (cf. Table 2). With regard to the anterior-posterior deviation, therefore it was sufficient to define the deviation only at the apices of kyphosis and lordosis, if necessary. In the example shown here it was −20 mm at T7.

Vertebrae with no prescribed deviation and/or rotation were free to move in all six degrees of freedom: lateral, anterior-posterior and inferior-superior translation, as well as rotations around the three principle axes. In addition to the prescribed deviation and/or rotation for some of the vertebrae, the others could be individually confined in any of their degrees of freedom by selecting corresponding tick boxes (Fig. 1b). Thereby individual vertebral bodies could be set fix in translation and/or rotation, if required.

The FEM simulation results from the ribcage model, according to the afore selected settings, were then shown together with the body scan image in the central section (B). Four subplots, and individual slicing of the images along the three principle axes allowed for an in-depth inspection in 3D (cf. B1), coronal (B2), transverse (B3) and sagittal (B4) view. The alignment of the body scan image relative to the simulated model and the scaling of the model could be adjusted by additional sliders and buttons (B5). According to the matching between the body contours and the simulated model deformation upon visual inspection, the initial settings could then be refined and displayed again until ribcage and spinal column are in anatomically and physiologically reasonable relation to the body contours throughout the whole body. The course of the spinal column depicted in the coronal view (B2) then corresponds to the spinal column seen in the anterior-posterior X-ray image.

Fig. 2 demonstrates at the examples of the same patient shown in Fig. 1a the effects of different parameter settings in several transverse, as well as coronal and sagittal cuts. While the centre column represents the optimum parameter setting, the left and right column show the effects of under- and overstated parameters at the example of longitudinal translation, Ty, and vertebral body rotation, Rz, respectively. An understated longitudinal translation, Ty, typically results in a partially off-centred

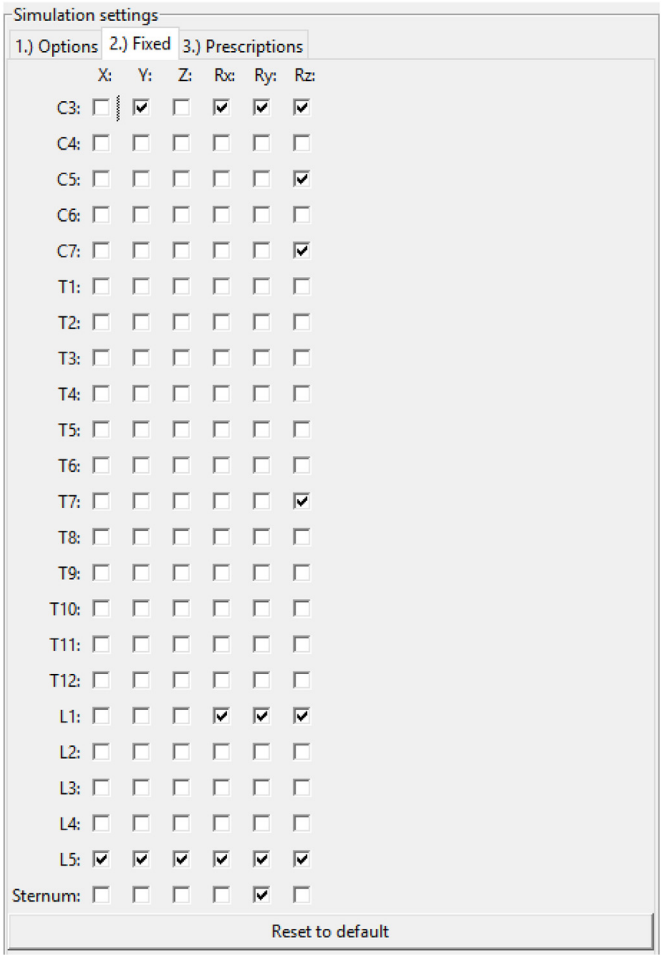

Figure 1. (*continued*).

model towards the front (highlighted region ① in 1st column) and potentially also an understated kyphose angle most clearly visible in the corresponding sagittal view (highlighted region ④ in 1st column). Accordingly an overstated Ty parameter leads to an off-centred model towards the back and an exaggerated kyphose angle, respectively (cf. highlighted regions ① and ⑤). In a similar manner an under-/overstated Rz becomes visible when comparing the back contours in the transverse cuts (cf. highlighted regions ②/③).

Further a so-called apex angle has been defined, in an attempt to transfer the results of the present methods and parameter settings into a measurement that also reflects the Cobb angle – a gold standard in X-ray analysis. The apex angle is defined as $180^\circ - \theta$, where θ is the included angle between the two legs from the main apex to the adjacent inflection points along the course of the vertebral column from back view [34]. In principle this apex angle can thus be derived both from images of coronal X-ray and from the back view of the model.

3. Results

In order to verify the reliability of the developed body scanner image analysis tools, we analysed twelve body scan images from ten patients, 5 female and 5 male. In terms of practical feasibility of the analysis tools, they provide an easy to use GUI to analyse 3D scan images from patients with spinal deformities by comparison with FEM simulations of the patient's specific geometry of ribcage and spinal column.

Fig. 3a and b show in summary the body scanner image analysis results of ten patients with spinal deformations, including two follow-up scans. Next to the patient IDs in the first column, X-ray images show the patient's individual spinal deformation in coronal view. The other subplots show the deformed spinal column and ribcage from FEM simulation results in posterior-anterior, sagittal and multiple transverse views, respectively, together with the body scan image (contours). In all cases reasonable good agreement were achieved between outer body contour and simulated ribcage and spinal column deformations from body scan and FEM simulation, respectively. While the posterior-anterior and sagittal views visualize the total spinal column and ribcage inside the body scan image, do the transverse cuts show the effects of lateral deviation and/or rotation on the apex level, but also their effects on other vertebral levels along the spine through the attached adjacent vertebral levels.

Table 2 lists the patient's data and the corresponding parameter settings used for the simulations. The parameter values of lateral and longitudinal deviations and rotations around the vertical body axis are relative values and thus indicate deviations of the vertebral bodies from their initial positions in non-deformed model configuration.

The Spearman rank-order correlation coefficient (ρ_s) between the Cobb angles and the lateral deviations Tx at main apex level is $\rho_s = 0.90$, with associated probability $p < 0.05$. Accordingly the correlation coefficient between the Cobb angles and the rotations (Rz) is $\rho_s = -0.87$ with $p < 0.05$. In general, the Spearman correlation coefficient is a measure of monotonicity of the relationship between two sets of data [49,50]. It can have values from $+1$ to -1. A ρ_s of $+1$, or -1, indicates a positive or inverse correlation, respectively, while ρ_s close to 0 would indicate no tendency for a relationship between the data. The p value is a probability that indicates statistical significance of a correlation coefficient value, when lower than the conventional 5%.

The apex angles from the coronal X-ray images and from the back views of the models upon simulation are listed in Table 3 along with the Cobb angles. The corresponding Spearman rank-order correlation coefficient value between the Cobb angles (CA) and the apex angles from coronal X-rays (APX) is $\rho_{CA-APX} = 0.89$ with $p < 0.05$. Accordingly the rank-order correlation coefficient values between the Cobb angles and the apex angles from the model (APM) were found to be $\rho_{CA-APM} = 0.68$ with $p < 0.05$ and $\rho_{APX-APM} = 0.71$ with $p < 0.05$ between both the apex angles.

In general, at the lower thoracic and thoraco-lumbar levels, the transverse cuts of the ribcage correspond in shape and size to the total outer contours of the body scan image, while at the upper thoracic levels the correspondence is given at the back and the centre of the front. Mild and medium spinal deformations, as shown here, overall seem to have rather small effect on the body contours at the front, if the back side is more heavily effected (e.g. Fig. 3a ID 07). Asymmetries between the left and right side, evident from a rib hump at the convex side of the back, are even more pronounced when there is distinct rotation around the vertical axis of the vertebrae involved (cf. Fig. 3b IDs 17, 21). The level of maximum asymmetry in the body contour, however, visibly may not always correspond to the apex level. In particular at the upper thoracic region, a pronounced asymmetry could be visible at the levels of the scapula, while the apex tend to be at a lower level. The anterior-posterior deviations towards ventral or dorsal are important to adjust the vertebral column to the dorsal line in sagittal view, but seem to have almost no effect on the asymmetry between left and right side of the body contours at the back in transverse view (cf. Fig. 3a IDs 04a/b).

4. Discussion

If scoliosis is suspected, regular clinical examinations are essential, especially for children in growing age. In addition to the clinical examination, X-rays are the gold standard to date. Alternative methods are important for a close monitoring without significant exposure to radiation though. Our present combined 3D body scanner image and ribcage

Table 2
Classification of patients' scoliosis evaluated from X-ray images and associated initial parameters for simulations.

ID:	Scoliosis range:	[a]Cobb angle [deg.]:	Nash-Moe index:	[b]Main apices & feature levels:	[c]Tx [mm]:	[c]Ty [mm]:	[c]Rz [deg.]:
02a	thoracic	+34	I	**T7**	29	5	−10
				L2	−7	−5	5
02b	thoracic	+20	I	**T7**	19	5	−8
				L2	−7	−5	
04a	thoraco-lumbar	+14	I	T7		−20	
				L1	20		−10
04b	thoraco-lumbar			T7		−35	
				L1	20		−10
06	thoracic	+12	I	T7		−10	
				T8	8		−5
				L2		5	
07	thoraco-lumbar	−12	I	T7	−9	−30	−5
				T12	−15		
16	lumbar	−14	I	T7	5	−15	−3
				L2	−8		
17	thoraco-lumbar	+15	I	T4			10
				T7		−20	
				T12	25		−20
18	lumbar	−16	I	T6	6		
				T7		−10	
				L1	−23		10
21	combined	+38/-33	II	T1	5		
				T7		10	
				T10	25		−25
				L2	−10	5	
22	thoraco-lumbar	−42	I	T7	5		−5
				T12	−15		10
27	lumbar	+10	I	T7		−20	
				L2	8		−10

[a] The sign of Cobb angle values corresponds to right (+) and left (−) convexity.
[b] Levels in **bold** font denote the apex level(s) of main curvature(s) in coronal view.
[c] Tx, Ty and Rz are relative values, indicating deviation from initial healthy configuration, where Tx: lateral deviation to left (−) and right (+); Ty: longitudinal deviation towards front (+) and back (−); Rz: rotation around the vertical body axis.

model analysis tools are a further step in this direction. The methods presented here, however, are not suitable to replace X-rays, rather than intended to provide supplementary information for an orthopaedic specialist especially when X-ray is not clearly justified.

The software enables an orthopaedic specialist in a decent manner of time to simulate and directly visualize different patient's specific spinal deformations inside the patient's body contours. Slicing from three different perspectives along the principle axes and the 3D view further allow for an in-depth inspection and analysis at any part of the trunk. The expenditure of time per patient, however, depends on multiple aspects. In general, the time needed to analyse a single body scan with body scanner image analysis tools increases with severity and complexity of the spinal deformation. In turn, the analysis time needed decreases with experience of the user and/or the availability of initial parameter values from X-ray, or previous body scan analysis. At present the X-ray image has to be available in DICOM format, because metadata like the pixel sizes are used to calculate the effective metric distances.

The body scan image analysis with the present tools are slightly more time-consuming than X-ray at the moment. While the overall scanning process is comparable or less time consuming than an X-ray, the iterative adjustment of the individual parameters during the analysis with body scanner image analysis tools takes more time than an X-ray assessment. On the other hand, the easy packaging and mobility of the body scanner and further developments towards a semi or fully automated fitting procedure have the potential to shorten the time required for a body scanner image analysis and are advantages over X-ray.

The patients analysed in this study had different types and severities of spinal deformations. The results show that the main field of application in clinical daily routine could be all types and severities of spinal deformations that require regular follow-up examinations, but not necessarily justify an X-ray.

The consideration of the age of the group in terms of a homogeneous group of patients are of no significance, since the aim of this study was to test whether our X-ray-free method can provide similar results to an X-ray image and provide supplementary information.

Given that spinal deformations seem to first show up at the transverse back contours, rather than at the front, good matching between the rib cage and body contours should be primarily achieved and rated according to the back side. In transverse cuts, the asymmetry between the left and right side of the back contour, in general, tend to show up rather at the thoracic and thoraco-lumbar regions, because of the ribcage and the ribs attached to the vertebral bodies, respectively. The effects of lumbar spinal deformations and apices below T12 then seem to propagate through the adjacent attached vertebrae to the ribcage and thereby become visible in the transverse body contours. Clear lumbar deformations, additionally, also show up in an asymmetric body contour in the posterior-anterior view similar to the waist asymmetry in clinical examination (cf. Fig. 3b ID 21). When adjusting the spinal configuration parameters – here Tx, Ty and Rz – the focus, however, should be on a parallel alignment of the transverse body contours to the transverse cuts of the ribcage, in particular at the back side and the centre of the front. The rather strong asymmetries in the scapula region, in comparison to lower levels, could be explained by a kind of enhancement effect. Here the ribs attached to the vertebral bodies lift the overlying scapula towards the back appearing in a more prominent asymmetry.

The inter- and intra-rater reliabilities are expected to be rather high, since human symmetry perception is fairly sensitive to identify already small asymmetries [51]. Fig. 2 shows that parameters values off the optimum results in effects clearly visible in transverse and sagittal and/or coronal view. Small inter- and intra-rater variabilities, however, are inherent to the present method, since it is partially based on manual interaction. A quantification of the inter- and intra-rater reliability will be possible upon further analysis with a larger number of patients and users. With further developments towards an automated routine for matching recognition, inter- and intra-rater reliability will be of minor relevance though.

The high Spearman rank-order correlation coefficient between the Cobb angles and lateral deviations indicates a strong relationship between these parameters. Similar the negative Spearman correlation coefficient close to −0.9 between the Cobb angles and the rotations indicates a strong inverse relationship. In either case thus significant correlations could be achieved, because the simulations are based on the combined effect of lateral deviation and rotation ($\Theta_{Cobb} \propto f(Tx, Rz)$). The number of samples is rather small though, which could affect the accuracy. Nevertheless, both parameters – lateral deviation and rotation – seem to be related to the Cobb angle and therefore could be used in a similar manner than the Cobb angle to characterise the severity of spinal deformation. Further, when comparing with previous simulation results, changes in any of these parameters are clear indications of a change in spinal course.

Similar there was found a very strong correlation between the Cobb and apex angles, shown by the high Spearman rank-order correlation coefficient value ($\rho_{CA-APX} = 0.89$) and small probability ($p < 0.05$). Although less strong, there also exist statistically significant ($p < 0.05$) strong correlations between the Cobb angles and the apex angles derived from the model calculations ($\rho_{CA-APM} = 0.68$), and between the apex angles from X-rays and the model calculations ($\rho_{APX-APM} = 0.71$), respectively. The very strong correlation between the Cobb and apex angles from X-rays suggests that the apex angle could potentially be used

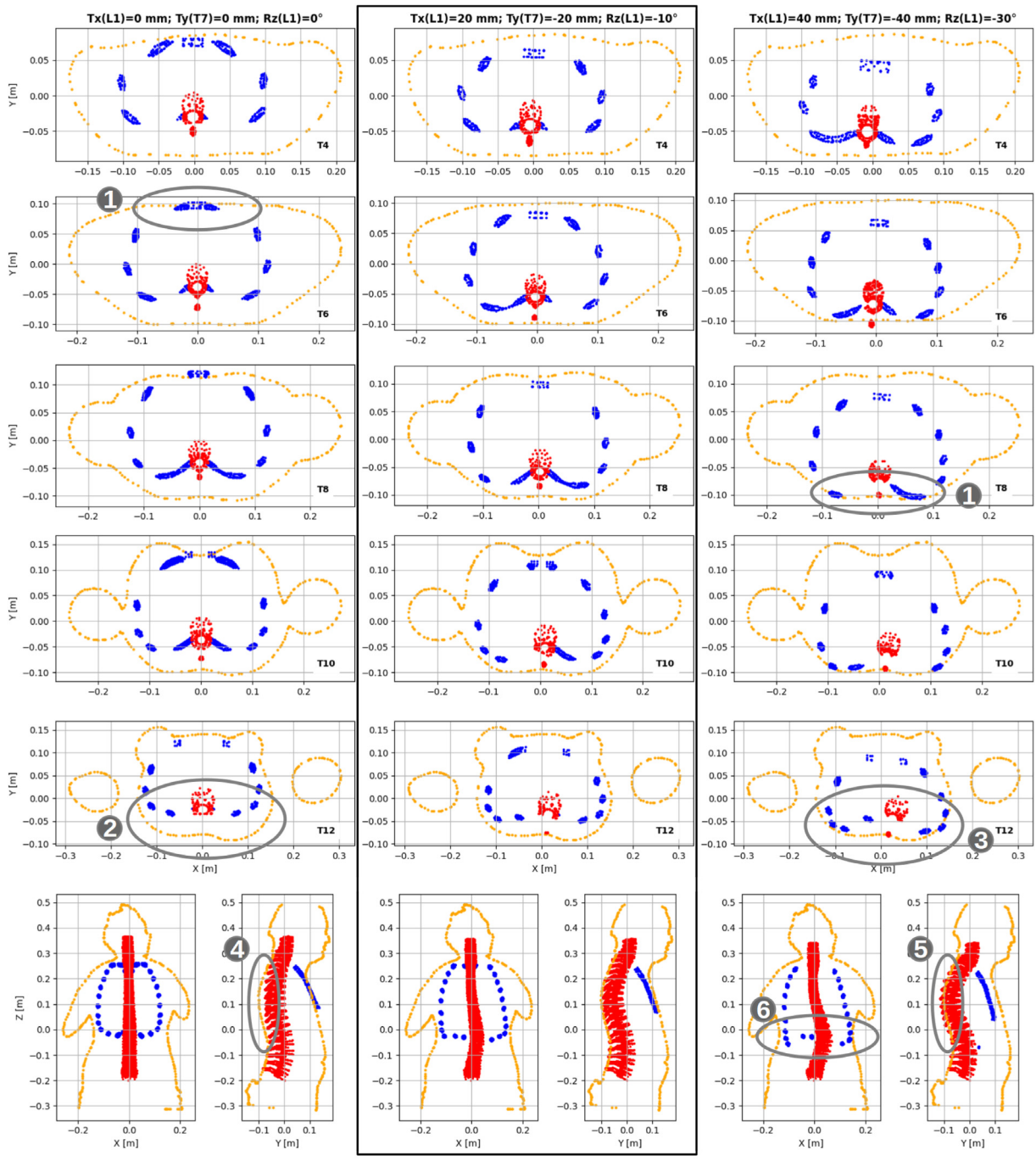

Figure 2. Transverse cuts of the body scan image and the ribcage and spine models at several levels in the thoracic spine region, as well as coronal and sagittal cuts, for three different parameter settings, with one per column. Highlighted regions and aspects show typical criteria when visually fitting the model into patient's body contours. While left and right column show extreme cases, the centre is best match.

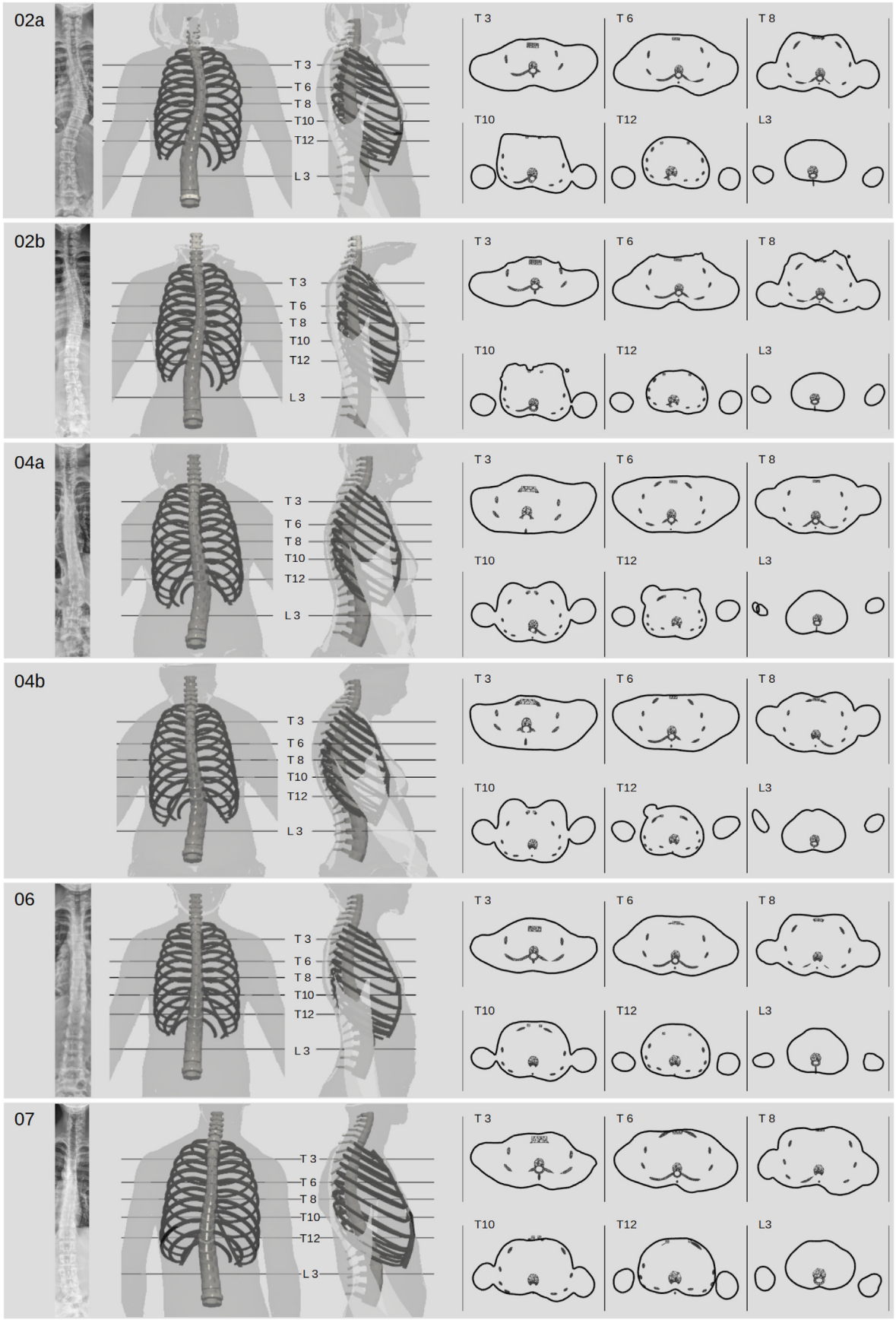

Figure 3. Fig. 3a: Patients images, showing from left to right: posterior-anterior X-ray, transparent bodyscans with simulated model inserted in back and sagittal view and corresponding transverse cuts. Each row represents different patients data. Numbers in first column correspond to patient ID. Letters in patient ID indicate follow-up images. Fig. 3b: Continuation of patient images (Fig. 3a).

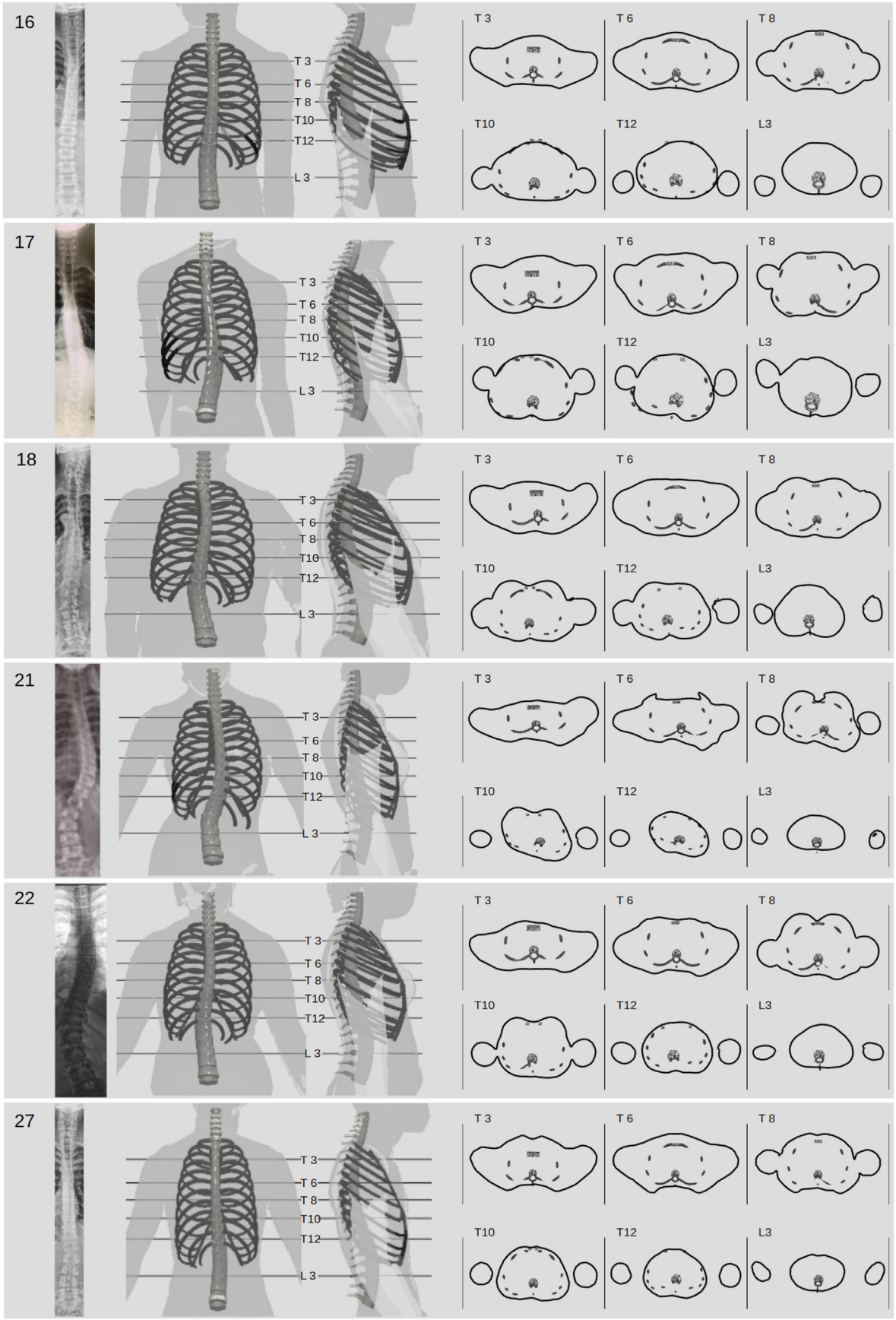

Figure 3. (*continued*).

Table 3
Apex angle values from both images of the coronal X-rays and models back views upon simulation.

ID:	[a]Cobb angle [deg.]:	Apex angle θ_{APX} [deg.]:	Apex angle θ_{APM} [deg.]:
02a	+34	26.8	15.4
02b	+20	20.7	11.5
04a	+14	12.5	17.9
04b			18.7
06	+12	7.0	0.0
07	−12	8.1	8.7
16	−14	6.8	10.1
17	+15	14.1	15.5
18	−16	20.6	15.7
21	+38/-33	29.6	23.3
22	−42	27.7	15.6
27	+10	10.3	9.5

[a] The sign of Cobb angle values corresponds to right (+) and left (−) convexity.

in complement to the Cobb angle for scoliosis assessment in follow-up examinations. With respect to its future application in clinical routine, the procedure of the present method could be as follows: When a patient exhibits signs of spinal deformation at its first clinical examination with an orthopaedic specialist, an X-ray examination will be performed according to the gold standard. In addition a 3D surface scan of the torso will be taken with the body scanner and from either image the apex angles will be extracted. Since the correlation coefficient value between the Cobb angle and the apex angle from X-ray was found to be significantly high, the apex angle then can be used for comparison in later follow-up examinations. At the next appointment with an orthopaedic specialist another body scan will be taken in addition to the clinical examination. The apex angle and parameter settings associated with the latest body scan then can be compared with the previous one(s) and thus in combination with the results from the clinical examination ease the decision whether another X-ray is indicated or not. If the results of the clinical examination and the present method show no, or only minor, changes, no X-ray may be required at this stage, thus reducing the exposure of ionizing radiation to the patient. While X-rays are necessary to see the curvature of the spine and to exclude the congenital spinal malformation, in particular at first examination, the present method has the potential to reduce the number of X-rays in follow-up examinations and thus reduce the accumulated doses of ionizing radiation over the life span of a patient.

At present the validity of the current method has to be continuously verified with increasing number of patients, before its translational application in clinical routine. Patients whose clinical examination reveals a spinal deformation and who requires an X-ray according to the orthopaedic specialist are asked to voluntarily have a body scan of their torso carried out. The present method and its results thereby directly can be compared with the corresponding X-ray, without exposing the patient to additional radiation. According to our assessment, determinants that may influence the validity of the present method currently are the biomechanical model and the fitting procedure of the distorted model inside the 3D body scan image of the torso. Future developments will therefore focus on an (semi–) automated recognition of anatomically good matchings between simulation results and body scan images. First tests based on next nearest neighbour distances between the ribcage (blue dots) and outer body contours (orange dots) in transverse planes – depicted in Fig. 4 by (grey) dotted straight lines – showed that the present software can be extended towards an automated matching recognition. Once an automated matching recognition is implemented, further iterative algorithms can be used to approach the optimum vertebral column configuration by automatically varying the parameter settings (Tx, Ty, Rz). Varying these parameters at certain key points (e.g. apex level(s)) will result in slightly different configurations with different matchings. The vertebral column configuration according to the best match settings is then expected to reflect the patients individual anatomical configuration.

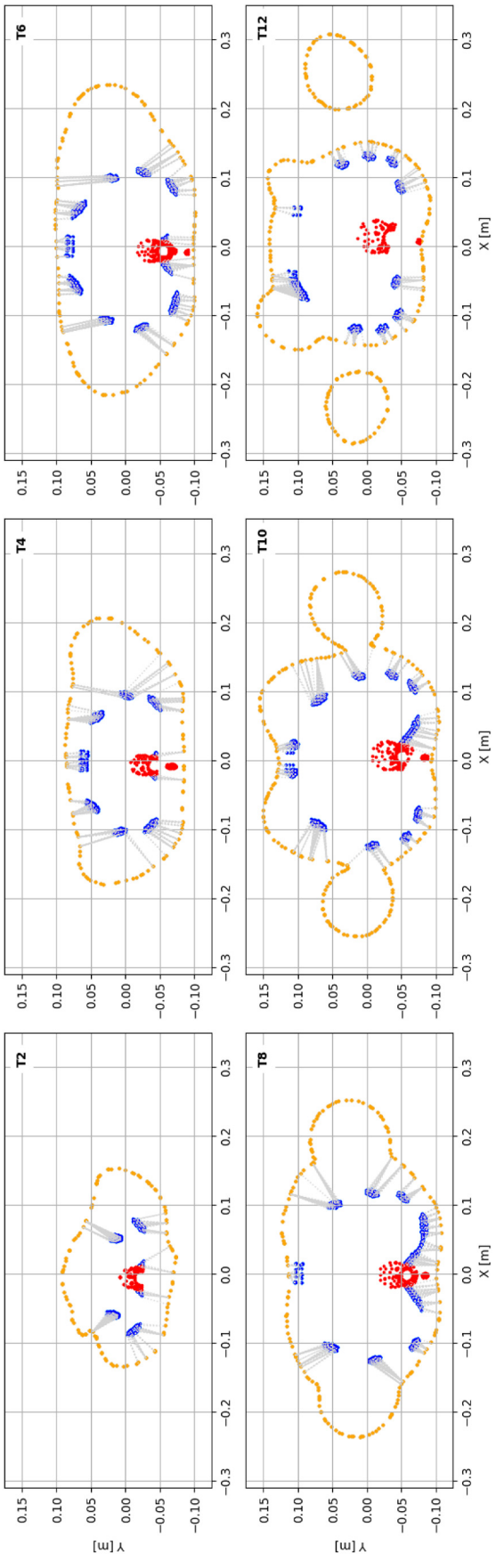

Figure 4. Transverse cuts of the body scan image (outer contour) and the ribcage and spine models at levels in the thoracic spine region. The distances between the ribcage and next nearest points in scan contours (gray lines) can be used to quantify the match between model and bodyscan, e.g. from standard deviation.

5. Conclusion

The body scanner image analysis tools presented here are intended to provide supplementary information for the assessment of spinal deformations in clinical daily routine, in order to reduce the number of X-rays in follow-up examinations. FEM simulations on biomechanical models of the spinal column and ribcage in combination with 3D images from a body scanner allow for an user-friendly visualization and easy slice-by-slice in-depths inspection of patient's specific spinal deformations from different perspectives without the use of ionizing radiation. Strong correlations between the Cobb angles and other parameters introduced in this paper suggest that the method might have the potential to be used for scoliosis assessment in follow-up examinations in complement to the Cobb angle.

Author contribution

Alexander T. D. Grünwald: Conception and design of study, acquisition of data, analysis and/or interpretation of data, Drafting the manuscript, Approval of the version of the manuscript to be published. **Susmita Roy:** acquisition of data, revising the manuscript critically for important intellectual content, Approval of the version of the manuscript to be published. **Renée Lampe:** Conception and design of study, acquisition of data, revising the manuscript critically for important intellectual content, Approval of the version of the manuscript to be published.

Funding

Financial supports from the Klaus Tschira Foundation (project N°.: 00.333.2017); Buhl-Strohmaier Foundation; and Würth Foundation are gratefully acknowledged by the authors.

Ethics declaration

Data were anonymous and all procedures were approved by the ethics committee of the Faculty of Medicine of the Technical University of Munich before starting the study.

Data availability

The data analyzed for the current study are available from the corresponding author on reasonable request.

Declaration of competing interest

The authors have no competing interests to declare that are relevant to the content of this article.

Acknowledgements

The authors would like to thank the participants for their time and support to this study.

References

[1] Stokes IA. Three-dimensional terminology of spinal deformity. a report presented to the scoliosis research society by the scoliosis research society working group on 3-d terminology of spinal deformity. Spine 1994;19:236–48.
[2] Lonstein JE. Adolescent idiopathic scoliosis. Lancet (London, England) 1994;344:1407–12.
[3] Smith JR, Sciubba DM, Samdani AF. Scoliosis: a straightforward approach to diagnosis and management. JAAPA : Off J Am Acad Physician Assistants 2008;21:40–5.
[4] Bettany-Saltikov J, Weiss H-R, Chockalingam N, Taranu R, Srinivas S, Hogg J, et al. Surgical versus non-surgical interventions in people with adolescent idiopathic scoliosis. The Cochrane database of systematic reviews; 2015CD010663.
[5] Asamoah V, Mellerowicz H, Venus J, Klöckner C. Oberflächenvermessung des rückens. Orthopä 2000;29(6):480–9. https://doi.org/10.1007/s001320050486.
[6] Oakley PA, Ehsani NN, Harrison DE. The scoliosis quandary: are radiation exposures from repeated x-rays harmful? Dose-Response 2019;17(2):1559325819852810. https://doi.org/10.1177/1559325819852810.
[7] Alzen G, Benz-Bohm G. Radiation protection in pediatric radiology. Dtsch Arzteblatt Int 2011;108(24):407–14. https://doi.org/10.3238/arztebl.2011.0407. arXiv:https://www.aerzteblatt.de/pdf.asp?id=93821, https://www.aerzteblatt.de/int/article.asp?id=93821.
[8] Presciutti SM, Karukanda T, Lee M. Management decisions for adolescent idiopathic scoliosis significantly affect patient radiation exposure. Spine J 2014;14(9):1984–90. https://doi.org/10.1016/j.spinee.2013.11.055.
[9] Zheng Y-P, Lee TT-Y, Lai KK-L, Yip BH-K, Zhou G-Q, Jiang W-W, et al. A reliability and validity study for scolioscan: a radiation-free scoliosis assessment system using 3d ultrasound imaging. Scoliosis Spinal Disorders 2016;11:13. https://doi.org/10.1186/s13013-016-0074-y.
[10] Knott P, Pappo E, Cameron M, deMauroy J, Rivard C, Kotwicki T, et al. Sosort 2012 consensus paper: reducing x-ray exposure in pediatric patients with scoliosis. Scoliosis 2014;9:4. https://doi.org/10.1186/1748-7161-9-4.
[11] Willner S. Moiré topography–a method for school screening of scoliosis., Archives of orthopaedic and traumatic surgery. Archiv Orthopadische Unfall-Chirurgie 1979;95:181–5.
[12] Turner-Smith AR. A television/computer three-dimensional surface shape measurement system. J Biomech 1988;21(6):515–29. https://doi.org/10.1016/0021-9290(88)90244-8.
[13] Oxborrow NJ. Assessing the child with scoliosis: the role of surface topography. Arch Dis Child 2000;83:453–5.
[14] Poredoš P, Čelan D, Možina J, Jezeršek M. Determination of the human spine curve based on laser triangulation. BMC Med Imag 2015;15:2.
[15] Drerup B. Rasterstereographic measurement of scoliotic deformity. Scoliosis 2014;9(1):22. https://doi.org/10.1186/s13013-014-0022-7.
[16] Grant CA, Johnston M, Adam CJ, Little JP. Accuracy of 3d surface scanners for clinical torso and spinal deformity assessment. Med Eng Phys 2019;63:63–71. https://doi.org/10.1016/j.medengphy.2018.11.004.
[17] Knott P, Sturm P, Lonner B, Cahill P, Betsch M, McCarthy R, et al. Multicenter comparison of 3d spinal measurements using surface topography with those from conventional radiography. Spine Deformity 2016;4:98–103. https://doi.org/10.1016/j.jspd.2015.08.008.
[18] Balla P, Manhertz G, Antal A. Diagnostic moiré image evaluation in spinal deformities. Opt Appl 2016;XLVI(3). https://doi.org/10.5277/oa160305.
[19] Roy S, Grünwald ATD, Alves-Pinto A, Lampe R. Automatic analysis method of 3d images in patients with scoliosis by quantifying asymmetry in transverse contours. Biocybern Biomed Eng 2020;40:1486–98. https://doi.org/10.1016/j.bbe.2020.09.001.
[20] Jaremko J, Delorme S, Dansereau J, Labelle H, Ronsky J, Poncet P, et al. Use of neural networks to correlate spine and rib deformity in scoliosis. Comput Methods Biomech Biomed Eng 2000;3:203–13.
[21] Al-Aubaidi Z, Lebel D, Oudjhane K, Zeller R. Three-dimensional imaging of the spine using the eos system is it reliable? a comparative study using computed tomography imaging. J Pediatr Orthoped Part B 2013;22:409–12. https://doi.org/10.1097/BPB.0b013e328361ae5b.
[22] Garg B, Mehta N, Bansal T, Malhotra R. Eos® imaging: concept and current applications in spinal disorders. J Clin Orthop Trauma 2020;11:786–93. https://doi.org/10.1016/j.jcot.2020.06.012.
[23] Tneb R, Seidl A, Hansen G, Pruett C. 3-d body scanning - systems, methods and applications for automatic interpretation of 3d surface anthropometrical data. Proc Hum Factors Ergon Soc Annu Meet 2000;44(38):844–7. https://doi.org/10.1177/154193120004403844. arXiv:.
[24] Schmitz A, Gäbel H, Weiß HR, Schmitt O. Anthropometrische datenerhebung mittels 3d-ganzkörperscan bei idiopathischer skoliose. Z Orthop Ihre Grenzgeb 2002;140(6):632–6.
[25] Li C, Zhang B, Liu L, Li Y, Xu Y, Wang L, et al. Design, reliability, and validity of a portable electronic device based on ergonomics for early screening of adolescent scoliosis. J Orthop Transl 2021;28:83–9. https://doi.org/10.1016/j.jot.2020.10.014.
[26] van der Plaats A, Veldhuizen AG, Verkerke GJ. Numerical simulation of asymmetrically altered growth as initiation mechanism of scoliosis. Ann Biomed Eng 2007;35:1206–15. https://doi.org/10.1007/s10439-007-9256-3.
[27] Aroeira RMC, Pertence AEM, Kemmoku DT, Greco M. The effect of hypokyphosis on the biomechanical behavior of the adolescent thoracic spine. J Braz Soc Mech Sci Eng 2018;40:128. https://doi.org/10.1007/s40430-018-1061-4.
[28] Dong E, Shi L, Kang J, Li D, Liu B, Guo Z, et al. Biomechanical characterization of vertebral body replacement in situ: effects of different fixation strategies. Comput Methods Progr Biomed 2020;197:105741. https://doi.org/10.1016/j.cmpb.2020.105741.
[29] Lasswell TL, Cronin DS, Medley JB, Rasoulinejad P. Incorporating ligament laxity in a finite element model for the upper cervical spine. Spine J 2017;17(11):1755–64. https://doi.org/10.1016/j.spinee.2017.06.040.
[30] Clin J, Aubin C-r, Lalonde N, Parent S, Labelle H. A new method to include the gravitational forces in a finite element model of the scoliotic spine. Med Biol Eng Comput 2011;49:967–77. https://doi.org/10.1007/s11517-011-0793-4.
[31] Wang W, Baran GR, Betz RR, Samdani AF, Pahys JM, Cahill PJ. The use of finite element models to assist understanding and treatment for scoliosis: a review paper. Spine Deformity 2014;2(1):10–27. https://doi.org/10.1016/j.jspd.2013.09.007.
[32] Cloake T, Gardner A. The management of scoliosis in children with cerebral palsy: a review. J Spine Surg 2016;2(4). URL, https://jss.amegroups.com/article/view/3684.

[33] Roy S, Grünwald ATD, Alves-Pinto A, Maier R, Cremers D, Pfeiffer D, et al. A noninvasive 3D body scanner and software tool towards analysis of scoliosis. BioMed Res Int 2019;2019:e4715720. https://doi.org/10.1155/2019/4715720. URL, https://www.hindawi.com/journals/bmri/2019/4715720/.
[34] Roy S, Grünwald ATD, Lampe R. Model-based radiation-free assessment of scoliosis: a principle validation study. J Med Biol Eng 2022. https://doi.org/10.1007/s40846-022-00678-8.
[35] Grünwald ATD, Roy S, Alves-Pinto A, Lampe R. Assessment of adolescent idiopathic scoliosis from body scanner image by finite element simulations. PLoS One 2021;16(2):e0243736. https://doi.org/10.1371/journal.pone.0243736. URL, https://journals.plos.org/plosone/article?id=10.1371/journal.pone.0243736.
[36] Maas SA, Ellis BJ, Ateshian GA, Weiss JA. FEBio: finite elements for biomechanics. J Biomech Eng 2012;134(1):011005. https://doi.org/10.1115/1.4005694.
[37] Gwinner J. Non-linear elastic deformations. Acta Appl Math 1988;11:191–3. https://doi.org/10.1007/BF00047287.
[38] Ogden RW. Non-linear elastic deformations. Mineola New York: Dover Publications Inc; 2013. URL, https://www.scribd.com/book/271533894/Non-Linear-Elastic-Deformations.
[39] Agnew AM, Moorhouse K, Kang Y-S, Donnelly BR, Pfefferle K, Manning AX, et al. The response of pediatric ribs to quasi-static loading: mechanical properties and microstructure. Ann Biomed Eng 2013;41:2501–14.
[40] Pezowicz C, Głowacki M. The mechanical properties of human ribs in young adult. Acta Bioeng Biomech 2012;14:53–60.
[41] Yang H, Jekir MG, Davis MW, Keaveny TM. Effective modulus of the human intervertebral disc and its effect on vertebral bone stress. J Biomech 2016;49(7):1134–40. https://doi.org/10.1016/j.jbiomech.2016.02.045.
[42] Zhu Y, Bermond F, Payen de la Garanderie J, Pialat J-B, Sandoz B, Brizard D, et al. In vivo assessment of elasticity of child rib cortical bone using quantitative computed tomography. Appl Bionics Biomechanics 2017;2017:e2471368. https://doi.org/10.1155/2017/2471368. URL, https://www.hindawi.com/journals/abb/2017/2471368/.
[43] Zhu Y, Fang Y, Bermond F, Bruyère-Garnier K, Ellouz R, Rongieras F, et al. Relationship between human rib mechanical properties and cortical bone density measured by high-resolution quantitative computed tomography. Comput Methods Biomech Biomed Eng 2013;16(sup1):191–2. https://doi.org/10.1080/10255842.2013.815888. arXiv:.
[44] Haverfield ZA. Quantifying variation in human rib volumetric bone mineral density (vbmd) and its relationship to fracture. Undergraduate Research Thesis. The Ohio State University; 2019.
[45] Deng Y-C, Kong W, Ho H. Development of a finite element human thorax model for impact injury studies. SAE Trans 1999;108:1193–9. URL, http://www.jstor.org/stable/44667989.
[46] Vanneuville G, Cluzel P, Massaux M, Bressolette P, Kyndt T, Garcier J, et al. A model of the human lumbar vertebral column: a preliminary study. Surg Radiol Anat 1995;17:53–7. https://doi.org/10.1007/BF01629500.
[47] Lan C-C, Kuo C-S, Chen C-H, Hu H-T. Finite element analysis of biomechanical behavior of whole thoraco-lumbar spine with ligamentous effect. Changhua J Med 2013;11:26–41.
[48] Lam GC, Hill DL, Le LH, Raso JV, Lou EH. Vertebral rotation measurement: a summary and comparison of common radiographic and CT methods. Scoliosis 2008;3:16. https://doi.org/10.1186/1748-7161-3-16. URL, https://www.ncbi.nlm.nih.gov/pmc/articles/PMC2587463/.
[49] Pirie W. Spearman rank correlation coefficient, vol. 8. John Wiley & Sons, Inc.; 2006. https://doi.org/10.1002/0471667196.ess2499.pub2.
[50] Zar JH. Spearman rank correlation: overview. John Wiley & Sons, Ltd; 2014. https://doi.org/10.1002/9781118445112.stat05964. arXiv:https://onlinelibrary.wiley.com/doi/pdf/10.1002/9781118445112.stat05964.
[51] Wagemans J. Characteristics and models of human symmetry detection. Trends Cognit Sci 1997;1(9):346–52. https://doi.org/10.1016/S1364-6613(97)01105-4.
[52] Forman JL, Kent RW. Modeling costal cartilage using local material properties with consideration for gross heterogeneities. J Biomech 2011;44(5):910–6. https://doi.org/10.1016/j.jbiomech.2010.11.034.